Antiresonant guiding in a poly(methyl-methacrylate) hollow-core optical fiber

2015 J. Opt. 17 105603

(http://iopscience.iop.org/2040-8986/17/10/105603)

IOP Publishing Journal of Optics
J. Opt. 17 (2015) 105603 (7pp) doi:10.1088/2040-8978/17/10/105603

Antiresonant guiding in a poly(methyl-methacrylate) hollow-core optical fiber

Christos Markos, Kristian Nielsen and Ole Bang

DTU Fotonik, Department of Photonics Engineering, Technical University of Denmark, DK-2800 Kgs. Lyngby, Denmark

E-mail: chmar@fotonik.dtu.dk

Received 24 April 2015, revised 24 June 2015
Accepted for publication 3 July 2015
Published 21 August 2015

Abstract

Strong antiresonant reflecting optical waveguiding is demonstrated in a novel poly (methyl-methacrylate) (PMMA) hollow-core fiber. The transmission spectrum of the fiber was characterized using a supercontinuum source and it revealed distinct resonances with resonant dips as strong as ~20 dB in the wavelength range 480–900 nm, where PMMA has low absorption. The total propagation loss of the fiber was measured to have a minimum of ~45 dB m^{-1} at around 500 nm. The thermal sensitivity of the fiber is 256 ± 16 pm $°C^{-1}$, defined as the red-shift of the resonances per °C, which is three times higher than the sensitivity of polymer fiber Bragg gratings.

Keywords: antiresonant guidance, polymer fiber, hollow-core fiber, fiber sensor

1. Introduction

The first hollow-core photonic crystal fiber (HC-PCF), demonstrating that >99.9% of the light can be guided in air, was presented in 1999 [1]. Since then there has been a tremendous interest from the scientific community in hollow-core fibers because they can be used in applications, such as gas, liquid and chemical sensing [2, 3], high-speed data transmission [4], terahertz guiding [5], and gas-based nonlinear optics [6, 7]. The confinement of light in a hollow-core fiber can be categorized into three main guidance mechanisms based on the structure of the fiber. The first type is the photonic bandgap mechanism under which the cladding, for a certain range of wavelengths, does not support modes with an effective refractive index around the refractive index of air [1]. Light in the core in those wavelength ranges is not able to couple to cladding modes and is consequently guided in the core with low losses [1]. The second mechanism does not support photonic bandgaps, but the core modes have a weak coupling with cladding modes. This is the so called 'low density of state guidance' or 'inhibited coupling' where the core modes and cladding modes have a low spatial overlap [8, 9]. A well-known example of such guidance is the Kagome fiber, where despite its higher propagation loss compared to the HC-PCF, Kagome fibers have a larger bandwidth [8–10]. The last main type of guiding mechanism is a simplified version of the two latter, where the light is confined in the core of the fiber via antiresonant reflecting optical waveguide (ARROW)[11, 12]. In this case, there are only discrete resonances in the cladding which will couple to the core modes. Although ARROW guidance has primarily been associated with hollow-core fibers, it has also been reported in solid-core PCFs, in both polymer and silica, where the cladding holes have been filled with high-index materials or high-index films [13–17].

Silica hollow-core antiresonant fibers have attracted significant attention recently because they can transmit light in the mid-IR transmission range with low loss. In 2011, Pryamikov *et al* experimentally presented the first hollow-core negative curvature ARROW fiber suitable for the spectral range 3–4 μm [18]. Belardi *et al* then demonstrated numerically a novel design of an antiresonant hollow core fiber with significantly reduced attenuation [19]. Since then several researchers have reported improved silica-based ARROW fibers mainly for the mid-IR spectral region. Antiresonant guiding has also been shown in the same spectral range using all-solid PCFs made by silver halide material [20]. However, limited research has been done in polymer hollow-core ARROW fibers [21, 22]. Polymer fibers are considered ideal candidates for sensing applications, such as temperature and strain sensing [23, 24] and fiber-optical biosensing [25–27] due to their high thermo-optic coefficient, low Young's modulus, and biocompatibility properties. In this work, we report on the fabrication of an ARROW fiber made of poly

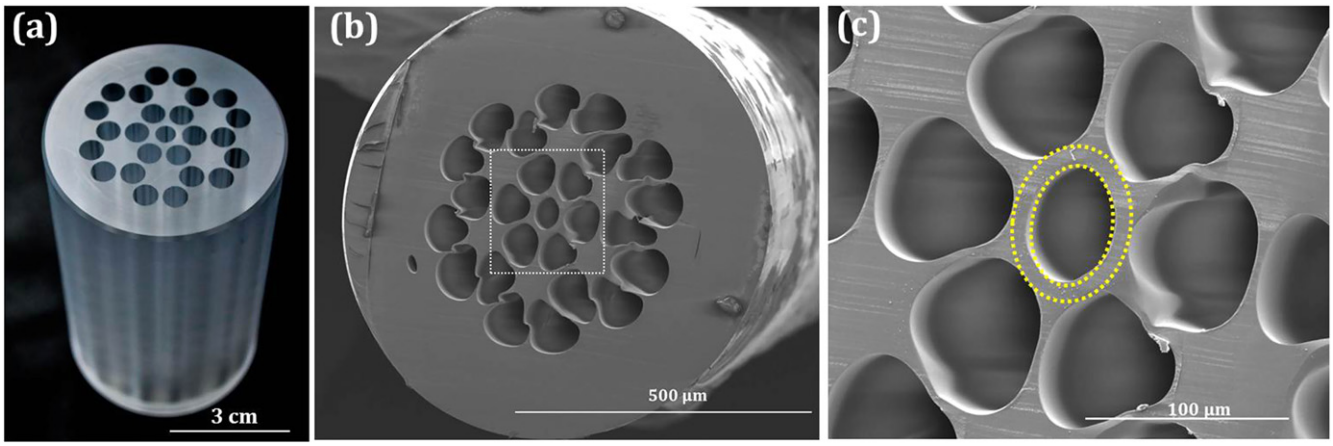

Figure 1. (a) Optical image of the initial preform of the fiber. (b) Scanning electron microscopy (SEM) image of the fabricated polymer hollow-core fiber. (c) Magnified SEM image of the core of the fiber with the yellow circles indicating the PMMA ring introducing the ARROW guidance.

(methyl-methacrylate) (PMMA) which constitutes a hollow-core and six-solid cores around it. The purpose of the proposed structure is that the surrounding solid cores can be used as high NA collector channels in sensing applications whilst further improvement of the robustness of the fiber to external mechanical perturbations is achieved. We show strong anti-resonant guiding with resonances as strong as 20 dB at 650 nm. The proposed fiber exhibits relative low loss compared to for example capillaries (~150 dB m^{-1} in the visible range with core size ~40 μm) [6], while the high thermo-optic coefficient of PMMA provides a thermal sensitivity of ~256 pm $°C^{-1}$. The proposed fiber structure has potential for fluorescence and Raman-based biosensing applications because the core modes could act as excitation source and the surrounding solid-cores could be used for collection of the fluorescent or Raman signal [28].

2. Fiber fabrication

The fiber was fabricated in-house using the drill-and-draw method. A primary PMMA cylindrical preform of diameter 6 cm and length 10 cm was drilled with the desired pattern using a computer controlled drilling machine as shown in figure 1(a). The preform was first drawn to a cane of ~5 mm diameter. The cane was sleeved with a single polymer tube and this secondary preform was then drawn to a ~730 μm in diameter fiber. Figure 1(b) shows a scanning electron microscopy (SEM) image of the end-facet of the fabricated fiber, which is seen to be slightly distorted due to the cleaving of the fiber. The fiber was cleaved using the hot-blade/fiber technique in order to obtain a good quality smooth surface. The temperature used for both the fiber and the cleaving blade was 77.5 °C, which has been shown to be optimum for cleaving PMMA PCFs [29]. The reason for this distortion, despite the optimum cleaving conditions, is that the structure of the fiber is composed of thin walls and thick polymer struts. Figure 1(c) shows a magnified SEM image of the core, where the thin polymer ring around the air core, which introduces the ARROW guidance, is indicated by yellow dashed circles. The diameter of the core of the fiber is ~43 μm.

However, it is important to stress, that the distortion does not proceed into the fiber, but is localized close to the end-facet, and does therefore not influence the guiding properties of the fiber. In order to verify that the distortion of the end facet of the fiber after cleaving does not proceed into the fiber, we observed the fiber from the side using an optical microscope. As it can be seen from figures 2(a) and (b), the distortion is superficial and does not propagate along the length of the fiber (~24 μm).

3. Optical characterization

For the optical characterization of the ARROW fiber, a supercontinuum laser source (SuperK Versa) was used, which covers the wavelength range from 500 to 2100 nm. The output beam from the laser was focused and coupled to a silica PCF (LMA-5) using a microscope objective in order to ensure single mode guidance coming out from the silica fiber for the full wavelength range. The output light from the silica PCF was then butt-coupled to the polymer ARROW fiber. The light was collected using a microscope objective and a multimode fiber and the transmitted signal was monitored on an optical spectrum analyzer. Any undesired light was blocked by inserting an iris diaphragm (with max diameter 20 mm) into the beam path, such that only light from the air core was recorded. A CCD camera was placed in the output path in order to record the near-field profile of the output of the fiber. The experimental set-up is shown in figure 3(a). Figure 3(b) shows the near-field with no light coupled to the fiber, while figure 3(c) shows the near-field when light is coupled into the air-core. Similarly, figures 3(d) and (e) show the near-field profiles when the light is coupled into a capillary and into the solid PMMA material around the core of the fiber, respectively.

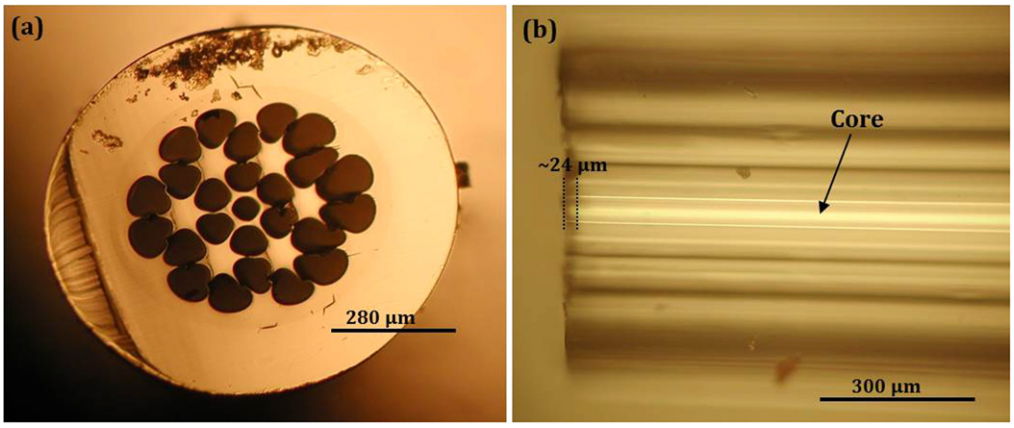

Figure 2. (a) Optical image of the cleaved end facet of the ARROW fiber. (b) Side view of the same fiber showing that the distortion of the microstructured area is local (30 um) and does not proceed along the length of the fiber.

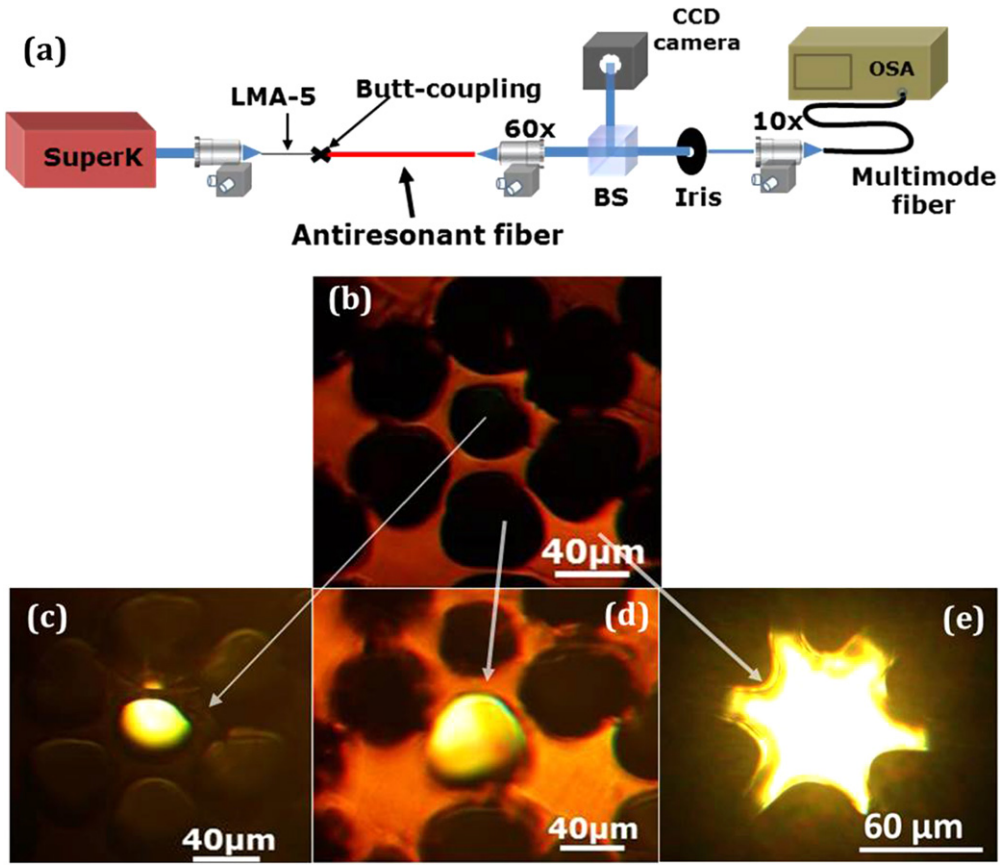

Figure 3. (a) Experimental set-up. Near-field profiles with (b) no light coupled to the fiber, (c) light coupled in the core of the fiber. (d), (e) Light was coupled in the capillary and solid bulk material next to the core, respectively.

ARROW guidance in a fiber is characterized by a number of minima and maxima in the transmission spectrum and occurs when the core, has a refractive index that is lower than the cladding. A thorough analysis of the ARROW mechanism has been extensively described elsewhere [12]. In our case, the low-index core is air and the high-index material is the PMMA ring around the core. As the light propagates along the fiber it interacts at a grazing incidence with the polymer walls and undergoes a resonant reflection (see inset of figure 3(b)). The resonant condition for the minimum transmission (on-resonance state) is given by [12, 30]:

$$\lambda_m = \frac{2n_1 t}{m}\left[\left(\frac{n_2}{n_1}\right)^2 - 1\right]^{1/2} = 1,\ 2,\ \ldots, \qquad (1)$$

where t is the thickness of the wall, n_1 and n_2 are the refractive indices of the low and high index materials (air and PMMA), respectively. These resonant wavelengths correspond to minima in the transmission spectrum. Figure 3(a) shows the normalized transmission spectrum of a 42 cm long

hollow-core fiber (black solid line). The spectrum reveals 12 distinct resonances over the visible spectral range 500–900 nm. The strongest resonances appear in the range ~600–700 nm and have a resonant depth of ~20 dB. Very recently, Rugeland *et al* demonstrated experimentally how the thickness of the wall determines the location of the resonances by etching a silica tube with 40% hydrofluoric acid [30]. Using equation (1), we calculate the location of the resonances by using the following values: $t = 5.4\ \mu$m, $n_1 = 1$ and $n_2 = 1.49$, where t is the estimated thickness of the PMMA ring around the core, n_1 is the refractive index of the core and n_2 is the refractive index of PMMA at 650 nm. The calculated locations of the minima are in good agreement with the measured spectrum and are shown in figure 4(a) (black spheres). The blue dotted line in figure 4(a) shows the spectrum recorded from one of the surrounding holes (see near-field profile in figure 3(d)). The transmission through the surrounding holes lack the resonance dips dominating the spectra from the central core. This is to be expected since the surrounding holes do not have a resonator ring around them and therefore can best be described as capillary waveguides. When the transmission spectrum of the hollow-core fiber (black solid line in figure 4(a)) is plotted in the frequency domain as seen in figure 4(b), the separation between the transmission peaks (maxima) is relatively constant [30].

In order to estimate the loss of the hollow-core ARROW fiber we made a cut-back measurement. The initial length of the fiber was 42 cm and after the cut the fiber length was 22 cm. Figure 5(a) shows the transmission spectra for the two lengths, i.e. 42 (black line) and 22 cm (red dashed line). The estimated propagation loss of the fiber is shown in figure 5(b). It can be seen that the minimum loss of ~ 45 dB m^{-1} was around 500 nm, which is for example lower than the loss of the first hollow-core microstructured polymer optical fiber (~55 dB m^{-1} at around 500 nm) [21]. It is well-known that the core size has crucial role for the loss of the fiber and thus it is important to emphasize that the core size of our fiber (~43 μm) is almost the same as the core size (~42 μm) of the fiber in [21]. Furthermore, the loss of the current fiber is significantly lower (~45 dB m^{-1} in the visible range) than a conventional capillary of similar core size (~150 dB m^{-1} in the visible range) [6]. Apart from the intrinsic confinement loss of the ARROW waveguide, additional sources of loss are scattering, in/out coupling losses and micro-bens introduced during the fabrication of the fiber. It should be noted that a long fiber and more than two cut-back points are necessary for an accurate measurement of the loss. However, due to the limited length of the fiber and the difficulties in cleaving the fiber, it was not feasible to measure additional cut-back points. It should be emphasized that the proposed fiber is mainly for applications where short lengths of fiber are required. The inset of figure 5(b) shows the connectorization of the proposed polymer hollow-core ARROW fiber with a conventional step-index silica fiber using UV-curable optical adhesive [32]. A first bonding between silica–PMMA was made with an optical UV-curable adhesive (NOA78-Norland) in order to have refractive index matching between the fibers and to avoid any kind of cavity effects. However, this

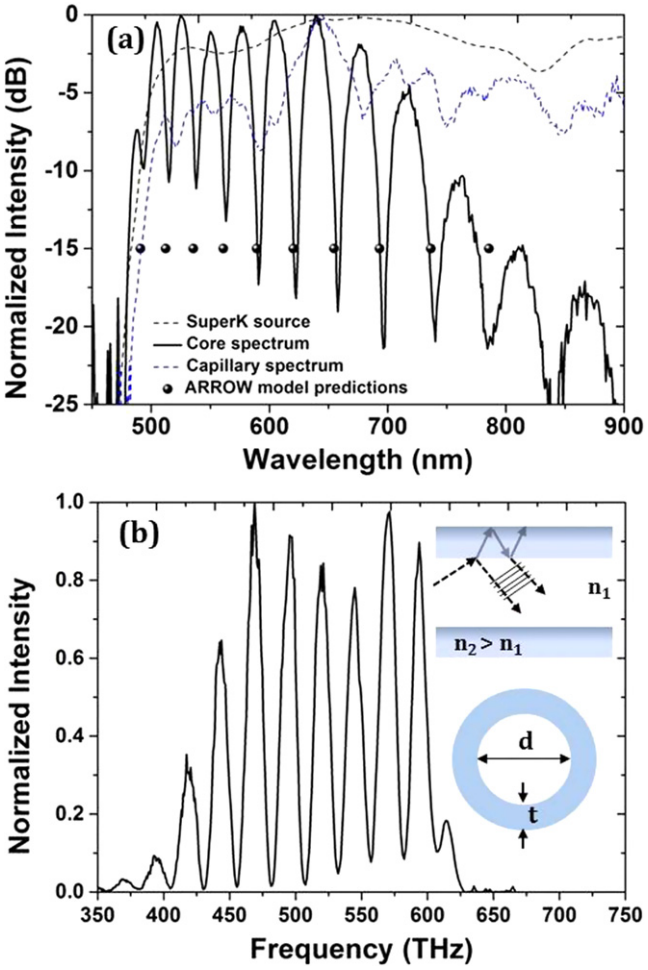

Figure 4. (a) Transmission spectrum of the hollow-core ARROW fiber (black line) and a neighboring capillary (blue dashed line). The spectrum of the SuperK source is given as a black dashed line. (b) Hollow-core ARROW fiber spectrum as a function of frequency showing periodic peak separation. Inset: schematic representation of the antiresonant reflection in the hollow-core fiber as the light interacts at a grazing incidence with the polymer walls.

adhesive has poor mechanical strength and therefore a second UV-curable adhesive was used to improve the robustness of the connection as also reported in [32]. This method has been used for most of fiber Bragg gratings (FBGs) polymer fiber sensors operating at 1550 nm [32] and it has been proven an efficient route for successful and robust connectorization of silica with polymer fibers when the loss of the fiber can be a limitation factor.

4. Temperature characterization

PMMA has a high thermo-optic coefficient ($\Delta n/\Delta T = -1.2 \times 10^{-4}$ at 633 nm) [31] compared to silica ($\Delta n/\Delta T = -2.5 \times 10^{-5}$ at 600 nm) [33] and therefore polymer fibers are well suited for sensing small temperature variations. Most polymer fiber temperature sensors are relying on FBG technology. The temperature sensitivity of an FBG in

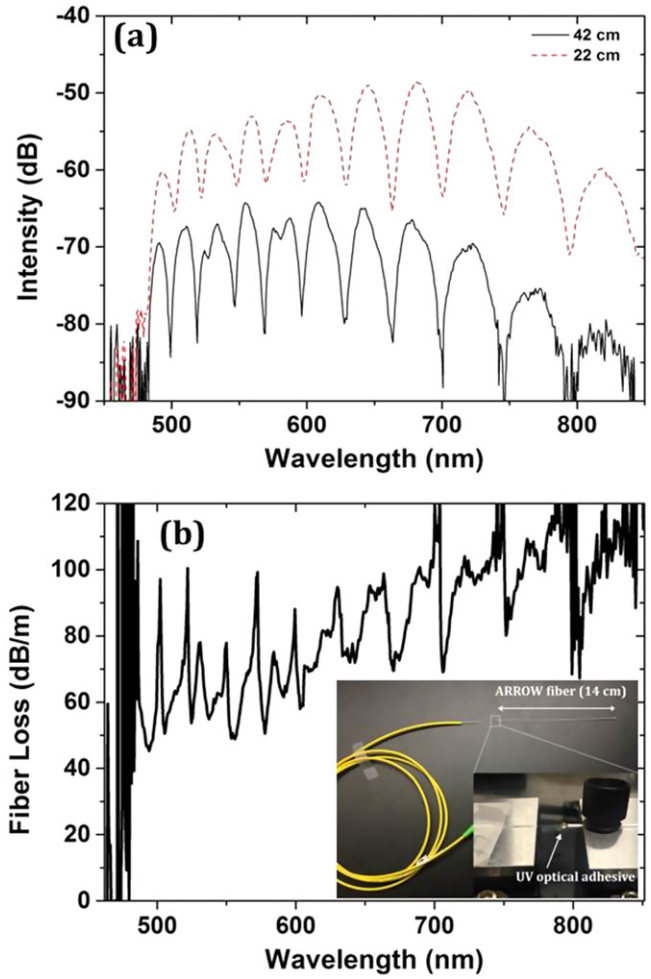

Figure 5. (a) Transmission spectrum of the 42 cm long fiber (black) and 22 cm long fiber (red). (b) Transmission loss of the hollow-core ARROW fiber based on a cut-back measurement with two cut-back points. Inset: connectorization of 14 cm long polymer hollow-core ARROW fiber with a conventional step-index silica fiber.

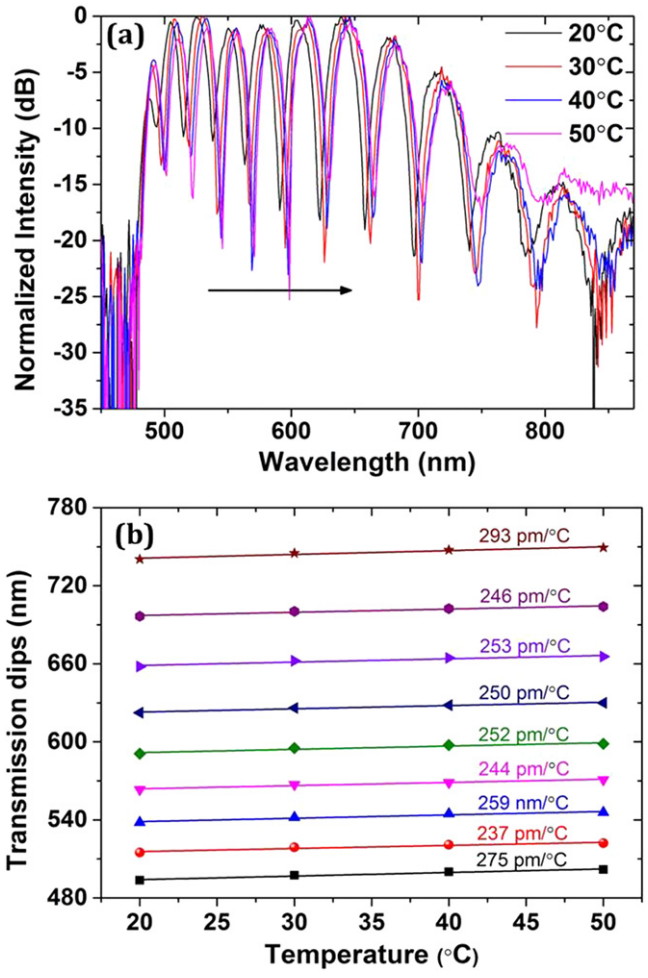

Figure 6. (a) Transmission spectrum of the ARROW fiber at different temperatures. (b) Dependence of the local transmission dips on temperature with the corresponding sensitivity given in the figure.

PMMA fibers has been reported to be in the range from −77 to −95 pm °C^{-1} [34]. For our temperature measurements, a controlled heating element (Linkam MC60) was placed in contact with the ARRROW hollow-core fiber. Figure 6(a) shows how the transmission spectrum red-shifts as the temperature increases from 20 to 50 °C. This wavelength red shifting can be explained mainly by the change of the thickness of the ring around the core due to the high thermal expansion coefficient of PMMA ($\sim 73.5 \times 10^{-6}$ °C) [35]. However, it should be emphasized that the thermally induced refractive index change of PMMA will also contribute to the change of the resonant dips. It has been already shown experimentally in polymer solid-core antiresonant fibers that when the temperature increases, the resonant dips are blue-shifting because the refractive index contrast between core and cladding is increasing (thermo-optic coefficient of polymer is negative) [15]. However, in our case, because the resonant dips are red-shifting with temperature instead of blue-shifting, allows us to conclude that the wall thickness expansion of the core dominates over the thermo-optic effect.

The shift of the resonances for 10 °C (figures 6(a) and (b)) was measured to be ∼6 nm. In order to match the 6 nm red-shift of the resonances with the ARROW model, the thickness of the PMMA wall estimated that it was expanded ∼ 70 nm based on the ARROW model as described in equation (1). Figure 6(b) shows how the location of the transmission dips depend on temperature. As it can be seen from figure 6(b), a relatively linear thermal response is observed for all the resonances (dips). The average temperature sensitivity of the ARROW fiber was found to be 256 ± 16 pm °C^{-1} which is higher than long period gratings in polymer fibers [36] and more than three times higher than the FBG response in polymer fibers [34]. This demonstrates that the proposed fiber potentially can be used as temperature sensor or tunable fiber-based optical filter for visible wavelengths.

5. Conclusion

In conclusion, we fabricated an ARROW fiber made of PMMA, which constitutes a hollow-core and six-solid cores around it. The spectral response of the fiber exhibited several

narrow resonances over the range 450–900 nm, due to the ARROW guiding characteristics. The minimum loss was estimated to be around $\sim 45\ \mathrm{dB\ m^{-1}}$ and the thermal sensitivity of the fiber was measured to be $256 \pm 16\ \mathrm{pm\ °C^{-1}}$. We demonstrate also that short lengths of the proposed ARROW fiber can be connectorized to a conventional step-index silica fiber using simply an optical adhesive. The main advantage of the proposed fiber is that it is fabricated using PMMA, which is biocompatible and suitable for *in vivo* biomedical applications. Also, the presented ARROW fiber could be used as a Raman or fluorescence probe for biosensing due to its hollow-core structure. The proposed fiber also opens the way for several other investigations, such as gas-based nonlinear effects, strain, and temperature sensing, as well as optofluidics applications.

Acknowledgments

The authors acknowledge the support from the Danish foundation 'Innovationsfonden' as part of the innovation consortium BIOFORS, contract no. 1382-00058B. C M would also like to acknowledge the Carlsberg Foundation and Hans Christian Ørsted post-doc program and for the financial support, Ivan-Lazar Bundalo for his help with the optical image of figure 1(a) and Alessio Stefani for fruitful discussions.

References

[1] Cregan R F *et al* 1999 Single-mode photonic band gap guidance of light in air *Science* **285** 1537–9
[2] Cox F M, Argyros A and Large M C J 2006 Liquid-filled hollow core microstructured polymer optical fiber *Opt. Express* **14** 4135–40
[3] Cubillas A M, Unterkofler S, Euser T G, Etzold B J, Jones A C, Sadler P J, Wasserscheid P and St. J. Russell P 2013 Photonic crystal fibres for chemical sensing and photochemistry *Chem. Soc. Rev.* **42** 8629–48
[4] Poletti F, Wheeler N V, Petrovich M N, Baddela N, Fokoua E N, Hayes J R, Gray D R and Richardson D J 2013 Towards high-capACity fibre-optic communications at the speed of light in vacuum *Nat. Photonics* **7** 279–84
[5] Anthony J, Leonhardt R, Leon-Saval S G and Argyros A 2011 THz propagation in kagome hollow-core microstructured fibers *Opt. Express* **19** 18470–8
[6] Travers J C, Chang W, Nold J, Joly N Y and St J Russell P 2011 Ultrafast nonlinear optics in gas-filled hollow-core photonic crystal fibers [Invited] *J. Opt. Soc. Am.* B **28** A11–26
[7] Benabid F, Knight J C, Antonopoulos G and St J Russell P 2002 Stimulated Raman scattering in hydrogen-filled hollow-core photonic crystal fiber *Science* **298** 399–402
[8] Argyros A and Pla J 2007 Hollow-core polymer fibres with a kagome lattice: potential for transmission in the infrared *Opt. Express* **15** 7713–77
[9] Wang Y, Wheeler N V, Couny F, Roberts P J and Benabid F 2011 Low loss broadband transmission in hypocycloid-core kagome hollow-core photonic crystal fiber *Opt. Lett.* **36** 669–71
[10] Markos C, Antonopoulos G and Kakarantzas G 2013 Broadband guidance in a hollow-core photonic crystal fiber with polymer-filled cladding *IEEE Photonics Technol. Lett.* **25** 2003–6
[11] Duguay M A, Kukubun Y, Koch T L and Pfeiffer L 1986 Antiresonant reflecting optical waveguides in SiO_2–Si multiplayer structures *Appl. Phys. Lett.* **49** 13–5
[12] Litchinitser N M, Abeeluck A K, Headley C and Eggleton B J 2002 Antiresonant reflecting photonic crystal optical waveguides *Opt. Lett.* **27** 1592–4
[13] Kuhlmey B T, Eggleton B J and Wu D K C 2009 Fluid-filled solid-core photonic bandgap fibers *J. Lightwave Technol.* **27** 1617–30
[14] Konidakis I, Zito G and Pissadakis S 2012 Photosensitive, all-glass $AgPO_3$/silicaphotonic bandgap fiber *Opt. Lett.* **37** 2499–501
[15] Yuan W, Wei L, Alkeskjold T T, Bjarklev A and Bang O 2009 Thermal tunability of photonic bandgaps in liquid crystal infiltrated microstructured polymer optical fibers *Opt. Express* **17** 19356–64
[16] Markos C, Yannopoulos S N and Vlachos K 2012 Chalcogenide glass layers in silica photonic crystal fibers *Opt. Express* **20** 14814–24
[17] Markos C, Kubat I and Bang O 2014 Hybrid polymer photonic crystal fiber with integrated chalcogenide glass nanofilms *Sci. Rep.* **4** 6057
[18] Pryamikov A D, Biriukov A S, Kosolapov A F, Plotnichenko V G, Semjonov S L and Dianov E M 2011 Demonstration of a waveguide regime for a silica hollow—core microstructured optical fiber with a negative curvature of the core boundary in the spectral region >3.5 μm *Opt. Express* **19** 1441–8
[19] Belardi W and Knight J C 2014 Hollow antiresonant fibers with reduced attenuation *Opt. Lett.* **39** 1853–6
[20] Lewi T, Ofek J and Katzir A 2013 Antiresonant reflecting microstructured optical fibers for the mid-infrared *Appl. Phys. Lett.* **102** 101104
[21] Argyros A, van Eijkelenborg M A, Large M C and Bassett I M 2006 Hollow-core microstructured polymer optical fiber *Opt. Lett.* **31** 172–4
[22] Argyros A, Leon-Saval S G, Pla J and Docherty A 2008 Antiresonant reflection and inhibited coupling in hollow-core square lattice optical fibres *Opt. Express* **16** 5642–56
[23] Webb D and Kalli K 2010 *Fibre Bragg Grating Sensors'* (Sharjah: Bentham eBooks) pp 293–4
[24] Dobb H, Webb D J, Kalli K, Argyros A, Large M C and van Eijkelenborg M A 2005 Continuous wave ultraviolet light-induced fiber bragg gratings in few- and single-mode microstructured polymer optical fibers *Opt. Lett.* **30** 3296–8
[25] Jensen J, Hoiby P, Emiliyanov G, Bang O, Pedersen L and Bjarklev A 2005 Selective detection of antibodies in microstructured polymer optical fibers *Opt. Express* **13** 5883–9
[26] Markos C, Yuan W, Vlachos K, Town G E and Bang O 2011 Label-free biosensing with high sensitivity in dual-core microstructured polymer optical fibers *Opt. Express* **19** 7790–8
[27] Emiliyanov G, Høiby P E, Pedersen L H and Bang O 2013 Selective serial multi-antibody biosensing with TOPAS microstructured polymer optical fibers *Sensors* **13** 3242–51
[28] Myaing M T, Ye J Y, Norris T B, Thomas T, Baker J, Wadsworth W J, Bouwmans G, Knight J C and Russell P S J 2003 Enhanced two-photon biosensing with double-clad photonic crystal fibers *Opt. Lett.* **28** 1224–6
[29] Stefani A, Nielsen K, Rasmussen H K and Bang O 2012 Cleaving of TOPAS and PMMA microstructured polymer optical fibers: core-shift and statistical quality optimization *Opt. Commun.* **285** 1825–33
[30] Rugeland P, Sterner C and Margulis W 2013 Visible light guidance in silica capillaries by antiresonant reflection *Opt. Express* **21** 29217–22

[31] Kang E-S, Lee T-H and Bae B-S 2002 Measurement of the thermo-optic coefficients in sol-gel derived inorganic-organic hybrid material films *Appl. Phys. Lett.* **81** 1438–40

[32] Stefani A, Andresen S, Yuan W, Herholdt-Rasmussen N and Bang O 2012 High sensitivity polymer optical fiber-bragg-grating-based accelerometer *IEEE Photonics Technol. Lett.* **24** 763–5

[33] Malitson I H 1965 Interspecimen comparison of the refractive index of fused silica *J. Opt. Soc. Am.* **55** 1205–8

[34] Yuan W, Stefani A, Bache M, Jacobsen T, Rose B, Herholdt-Rasmussen N, Nielsen F K, Sorensen O B, Hansen K S and Bang O 2011 Improved thermal and strain performance of annealed polymer optical fiber bragg gratings *Opt. Commun.* **284** 176–82

[35] Haward R N and Trainor A 1974 The thermoelastic effect in PMMA *J. Mater. Sci.* **9** 1243–54

[36] Argyros A 2013 Microstructures in polymer fibres for optical fibres, thz waveguides, and fibre-based metamaterials *ISRN Optics* **2013** 785162